ELSEVIER

Earth and Planetary Science Letters 203 (2002) 621–634

EPSL

www.elsevier.com/locate/epsl

How to anchor hotspots in a convecting mantle?

Anne Davaille *, Fabien Girard, Michael Le Bars

Laboratoire de Dynamique des Systèmes Géologiques, IPG, 4 Place Jussieu, 75252 Paris Cedex 05, France

Received 24 January 2002; received in revised form 26 July 2002; accepted 2 August 2002

Abstract

Laboratory experiments were performed to study the influence of density and viscosity layering on the formation and stability of plumes. Viscosity ratios ranged from 0.1 to 6400 for buoyancy ratios between 0.3 and 20, and Rayleigh numbers between 10^5 and 2.10^8. The presence of a chemically stratified boundary layer generates long-lived thermochemical plumes. These plumes first develop from the interface as classical thermal boundary layer instabilities. As they rise, they entrain by viscous coupling a thin film of the other layer and locally deform the interface into cusps. The interfacial topography and the entrainment act to further anchor the plumes, which persist until the chemical stratification disappears through entrainment, even for Rayleigh numbers around 10^8. The pattern of thermochemical plumes remains the same during an experiment, drifting only slowly through the tank. Scaled to an Earth's mantle without plate tectonics, our results show that: (1) thermochemical plumes are expected to exist in the mantle, (2) they could easily survive hundreds of millions of years, depending on the size and magnitude of the chemical heterogeneity on which they are anchored, and (3) their drift velocity would be at most 1–2 mm/yr. They would therefore produce long-lived and relatively fixed hotspots on the lithosphere. However, the thermochemical plumes would follow any large scale motion imposed on the chemical layer. Therefore, the chemical heterogeneity acts more as a 'floating anchor' than as an absolute one.
© 2002 Elsevier Science B.V. All rights reserved.

Keywords: mantle plumes; convection; mixing; thermochemical properties

1. Introduction

Long intraplate volcanic tracks like the Emperor–Hawaiian chain can be explained by the motion of plates above stationary 'hotspots' [1]. Hotspots can remain active for more than 120 Myr and they move laterally much more slowly than the lithospheric plates [2,3]. Most of these hotspots could be produced by the impingement on the lithosphere of hot and narrow plumes rising from a deep mantle boundary layer [4]. Isolated plumes coming from a localized source of buoyancy (either thermal or compositional) have been extensively studied (e.g. [5–10]) and have been shown to explain quantitatively a number of hotspot features such as the dynamic swell [11,12] or the volume ratio between head/flood basalts and stem/island chain [6,13]. However, to generate these fixed, long-lived plumes from a thermal boundary layer heated over its entire area is not so easy [14]. Applied to the Earth's mantle, the

* Corresponding author. Tel.: +33-1-44-27-23-22-38; Fax: +33-1-44-27-24-81.
E-mail address: davaille@ipgp.jussieu.fr (A. Davaille).

0012-821X/02/$ – see front matter © 2002 Elsevier Science B.V. All rights reserved.
PII: S0012-821X(02)00897-X

scaling laws derived in a homogeneous fluid for thermal convection in the plume regime (e.g. [15]) predict convective instabilities issuing from the lower hot boundary layer that are too weak and too short-lived. The temperature dependence of the mantle rheology further increases this tendency [16] as well as the presence of internal heating [17], so that these hot plumes should not even reach the lithosphere. These inferences apply to a convecting mantle in the absence of plate tectonics. The situation is even worse if we consider the 'mantle wind' created by plate motions which further acts to shear the plumes [6,18–20]. It is often argued that plume fixity could result from an increase of viscosity in the lower mantle or from a decrease of the thermal expansion coefficient at the bottom of the lower mantle [21], but another problem then arises: many mantle plumes (e.g. Hawaii) are too cold to have arisen from a purely thermal core–mantle boundary layer having the expected temperature jump ($\sim$1000°C) [9,10] and others are too weak to have traversed the entire depth of the mantle [9]. So, as this brief review shows, we need a mechanism to produce plumes not too hot nor too weak to produce hotspots, and to 'anchor' them in a convecting mantle.

Using laboratory experiments, Namiki and Kurita [22] showed that topography of sufficient amplitude on an interface deep in the mantle might fix the location of a hot plume in time-dependent convection. On the other hand, both geochemical and seismological data show that the mantle is heterogeneous in density on a large range of length scales. Hotspots themselves sample mantle geochemical reservoirs distinct from those sampled by mid-ocean ridges (e.g. [23]). Albers and Christensen [9] and Farnetani [10] showed that the temperature anomaly associated with a plume generated from a thermal boundary layer stratified in density could be much reduced. Studying the interaction of thermal convection with a stratification in density and in viscosity, Davaille [24,25] further showed that the presence of a thermochemical boundary layer at depth in the mantle would produce long-lived thermochemical plumes, provided that the local buoyancy ratio, the ratio of the chemical density anomaly $\Delta\rho$ to the thermal density anomaly across the interface, was greater than a critical value.

In Section 2, we further detail the characteristics of these plumes (origin, geometry, temperature anomaly, duration), using three sets of experiments on thermochemical convection (Fig. 1). Two of them (shown in Fig. 1a,c) have already been detailed elsewhere [24–26] and will just be briefly reviewed. The third set of experiments was designed to identify and study more easily

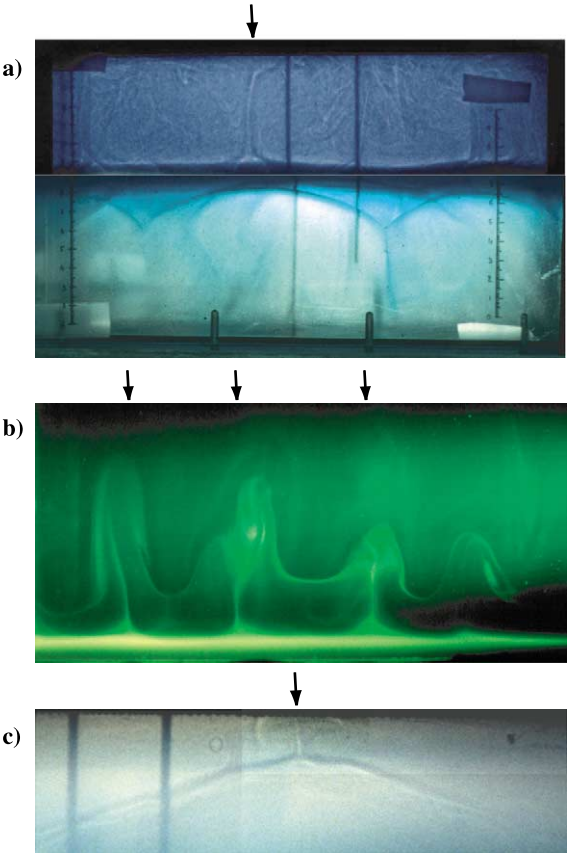

Fig. 1. Three ways to create a thermochemical plume (shown by an arrow). (a) Out of the interface in stratified convection: $B=2.4$; $\gamma=90$; $Ra=6.4\times10^7$; $a=1$ (shadowgraph showing the refraction index gradients associated with temperature and composition gradients). (b) From a stratified thermal boundary layer: $B=0.41$; $\gamma=30$; $Ra=9\times10^6$; $a=15$ (the thin denser layer is dyed with fluorescein). (c) Out of the top of a dome: $B=0.2$; $\gamma=18$; $Ra=1.1\times10^7$; $a=3$ (shadowgraph).

the thermochemical plumes, and involved convection above or below a thin non-convecting layer of fluid, which can be either less viscous or more viscous than the convecting layer [27,28]. They enabled us to determine the influence of the viscosity ratio on the entrainment rate and on the duration of thermochemical plumes. The scaling laws derived from the experiments are then extrapolated to the Earth's mantle in Section 3.

2. Three-dimensional thermochemical plumes in laboratory experiments

2.1. Experimental procedure

Two superposed layers of viscous fluid, initially isothermal at T_0, were suddenly cooled from above and heated from below in a Plexiglas tank. In the experiments reported here, the initial density and viscosity stratifications were sharp. The fluids were mixtures of water, salt, and cellulose (trade name 'Natrosol'), with concentrations independently varied to obtain initial density differences between 0.03 and 4%, and viscosity ratios γ between 0.095 and 6×10^4. The Prandtl numbers in each layer were always greater than 100, ensuring that inertial effects were negligible [29]. The liquids are miscible in all proportions and the temperature dependence of the viscosity (at most a factor of 2 across the whole tank) is negligible compared to its composition dependence. The lower layer was always the most viscous. Diffusion of Natrosol at the interface is inexistent whereas the high viscosities render diffusion of salt extremely slow compared to the characteristic time scale of the instabilities [25]. One of the layers was dyed to facilitate visualization. The convective motions were followed with shadowgraph and laser-induced fluorescence images. Heat and mass transfer were monitored through time by measuring temperature profiles and the densities of both layers.

2.2. Parameters

In our discussion, layer 2 designates the one with the higher Rayleigh number, since we focus on three-dimensional thermochemical plumes, which develop from the thermochemical interface in the most active layer [24,25]. Apart from the Prandtl number, five dimensionless numbers characterize each experiment:

- the Rayleigh number $Ra=(\alpha g\Delta T d^3/\kappa\nu_2)$, where d is the tank depth, ΔT is the temperature difference applied across it, g is the gravitational acceleration, α is the thermal expansivity at layer 2 mean temperature, κ is the thermal diffusivity and ν_2 is the kinematic viscosity of layer 2. This Rayleigh number is always greater than 10^5, which ensures the development of thermal plumes in layer 2 [29].
- the viscosity ratio $\gamma=\nu_1/\nu_2$, which ranged from 9.5×10^{-2} to 6×10^4.
- the depth ratio $a=d_2/d_1$, which ranged from 1 to 28.6.

Table 1
List of experiments

#	Ra	B	γ	a	L/d	t_{end} (min)	δ_{meas} (mm)	δ_{cal} (mm)	d_1/δ_{cal}	Ra_c
8	2.4×10^8	2.10	193	11.3	5	1056	-	-	-	-
10	4.6×10^5	2.70	15	5.15	5	630	20 ± 4	19.7	0.504	919.8
20	7.0×10^5	2.47	24	10.15	5	140	17 ± 2	13.6	0.403	939.0
30	1.5×10^6	4.46	51.5	11.20	5	220	14.9	11.0	0.456	942.6
40	9.2×10^5	0.35	38	6.7	5	65	15.3	15.8	0.505	935.4
60	1.15×10^6	2.59	59.5	9.25	5	NC	16.6	12.7	0.473	945.4
100	1.1×10^6	1.63	0.095	11.3	5	90	14.5	14.2	0.351	566.8
200	1.25×10^7	1.90	0.095	20.15	2	81	18.6	18.6	0.376	564.5
300	1.3×10^7	2.10	30	13.8	2	800	20.3	18.3	0.547	931.1
310	9.2×10^7	2.67	263	8.6	2	1560	15.6	14.7	0.680	945.9
320	6.1×10^6	1.63	0.447	11.33	2	150	20.7	17.7	0.280	711.4

- the aspect ratio L/d. Two tanks were used with a depth of 148 mm and 61 mm, respectively, which leads to aspect ratios of 2 and 5.
- the buoyancy ratio $B=(\Delta\rho/\rho\alpha\Delta T)$. This is the key parameter in determining the convective regime [26,27,30,31]. For B lower than a critical value B_c, the interface deforms in large domes which move up and down quasi-periodically in the whole tank (Fig. 1c), while for $B>B_c$, thermal convection develops in two superimposed layers, separated by a thermal boundary layer at a relatively undeformed interface. There, the interaction of thermal convection with the stratification produces thin thermochemical plumes that live much longer than pure thermal instabilities. B_c is a weak function of a and γ, and typical values of B_c are between 0.2 and 0.5 [24,26].

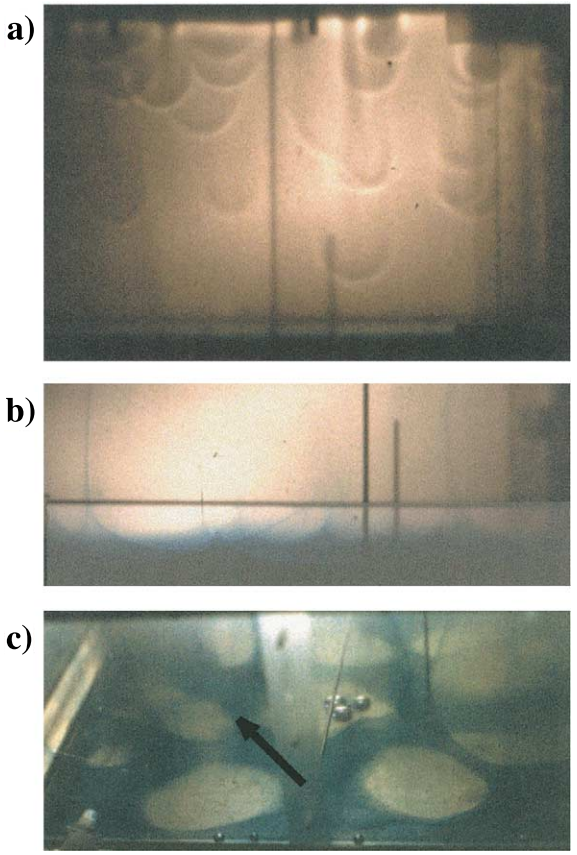

Fig. 2. Snapshots of RUN #320 (the thin layer is less viscous) through time. The thin layer is dyed blue. (a) 8.5 min, shadowgraph showing the onset of purely thermal plumes. Horizontal and black thick lines are the thermocouple probes. (b) 32 min, the interface deforms into cusps and thin blue filaments are entrained in the thermochemical plumes. (c) 123 min, the thin layer is eroded; the arrow indicates the drift direction of the whole pattern.

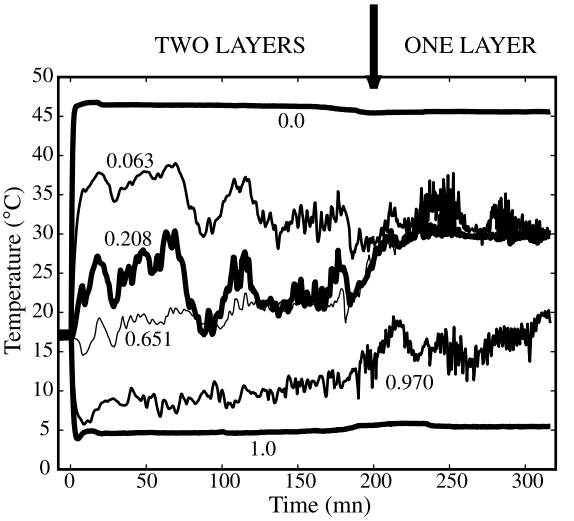

Fig. 3. Evolution through time of the temperature taken at different depths given in z/d. RUN #30 (the thin layer is more viscous).

The characteristics of the experiments with only one layer convecting above or below a thin layer are given in Table 1, while the details on the cases where both layers convect can be found in Davaille [25].

2.3. Results with a thin layer ($a>5$)

Here, one layer is too thin to convect (Table 1). Since the lower layer is the most viscous one, the thin layer (layer 1) is either the lower hot and viscous one ($\gamma>1$) or the upper cold and less viscous one ($\gamma<1$), but since the viscosity does not depend on temperature, the two situations are physically equivalent and up and down can be reversed. For the sake of simplicity, we will therefore always discuss the thermochemical plumes as if they are 'rising' from an interface.

2.3.1. Thermal plumes

The first convective motions to develop are always plumes generated from the thermal bound-

ary layer on the outer boundary of layer 2. The typical length scale of these instabilities is 1–3 cm (Fig. 2a). They correspond to a purely thermal mode of convection at high Rayleigh number: the thermal boundary layer grows steadily by heat diffusion until it reaches a critical size above which it is unstable; a thermal is then emitted, flushing the boundary layer, and the process repeats itself. The lifetime of these thermal plumes is quite short, typically 5–10 min. Although there is no coherent flow on the scale of the whole tank, plume formation at one given location is nearly cyclic and the amplitude of the associated thermal anomaly is small (Fig. 3). The plumes are not buoyant enough to substantially deform the interface when they reach it. Their onset time and periodicity are given by [15]:

$$\tau_c = \frac{d_2^2}{\pi\kappa}\left(\frac{Ra_c}{Ra_2}\right)^{2/3} \quad (1)$$

where $Ra_2 = (\alpha_2 g \Delta T_2 d_2^3/\kappa\nu_2)$, ΔT_2 is the temperature drop across the outer thermal boundary layer, α_2 is the mean value of the thermal expan-

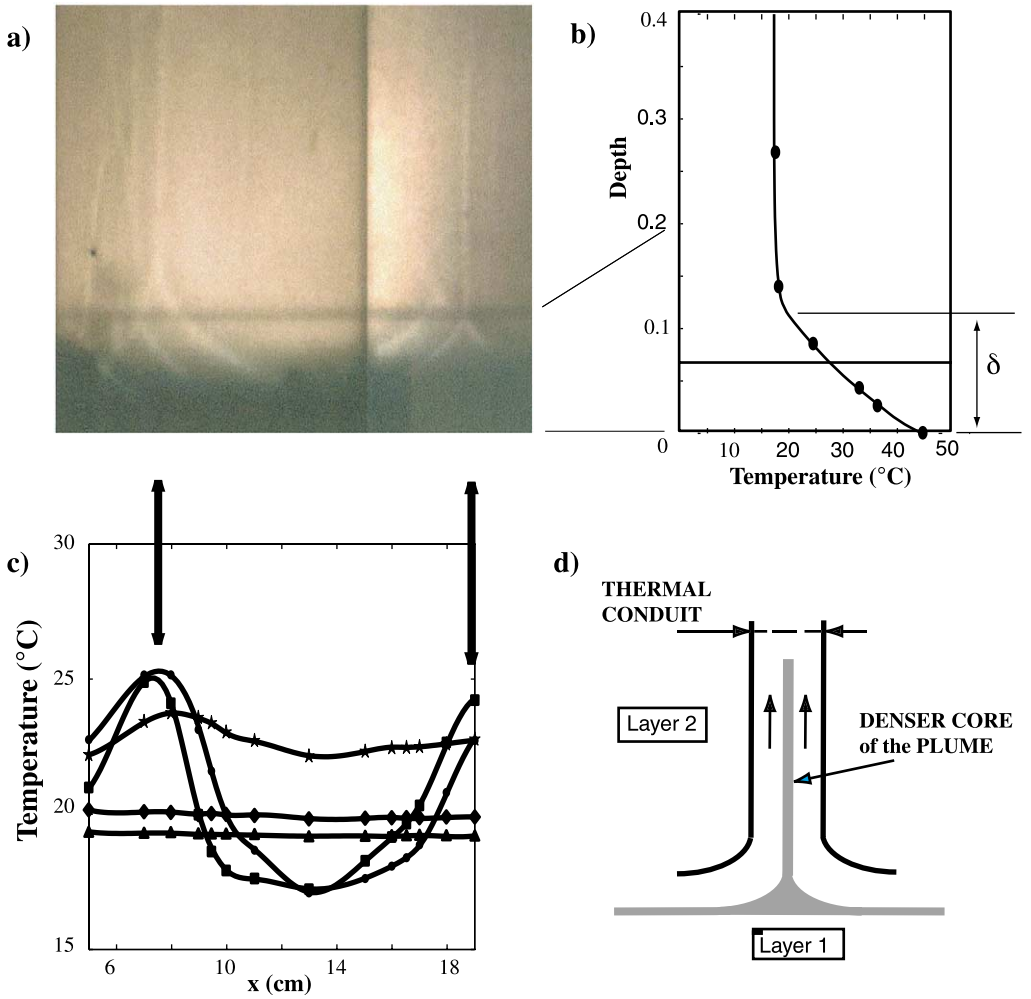

Fig. 4. Onset of thermochemical plumes in RUN #300 (the thin layer is more viscous). (a) Shadowgraph; (b) vertical temperature structure at $t = 22$ min; (c) horizontal temperature structure at $z/d = 0.2$ for different times (triangles, $t = 0$; diamonds, 9 min; stars, 14 min; disks, 19 min; squares, 22 min); (d) sketch of a thermochemical plume.

sivity across it, and $Ra_c = 1170 \pm 400$ is an experimental constant [32]. This thermal mode persists during the whole experiment.

2.3.2. Thermochemical plumes

2.3.2.1. Description. On the side of layer '1', it takes longer to develop any instabilities. A thermal boundary layer develops by conduction from the thermostated copper plate (Figs. 4 and 5). Then, the interface suddenly undulates, before deforming into cusps from which thin filaments are entrained by instabilities rising from the interface (Figs. 1b and 2b). The instabilities proceed out as triple or quadruple junction (Fig. 2b) of a branched network of vertical sheet-like structures (Fig. 1b) before becoming axisymmetric away from the interface [33–36]. Fig. 4c shows several horizontal temperature profiles around the onset time, where the horizontal probe was aligned with one of these vertical sheets. The probe records an increase in temperature on its whole length, before the two hot anomalies emerge. Note also that the thermal heterogeneity associated with each plume (Fig. 4c) is much wider than the entrained filament itself (Fig. 4a). A thermochemical plume is therefore constituted mostly of buoyant material from layer 2 plus a thin core of layer 1 (Fig. 4d). The amplitude of the plume temperature anomaly is typically 0.40 of the temperature difference across the thermochemical boundary layer ΔT_B (Fig. 4b), being maximum at the interface, and correlated vertically over the whole tank. These big thermal anomalies generate heat flux heterogeneities as much as four times bigger than the heat flux produced by purely thermal convection.

The thermochemical plumes form a stable polygonal pattern (reminiscent of the 'spoke' pattern) which sometimes drifts slowly throughout the experiment. The topography of the interface follows this pattern, with material piling up under each thermochemical plume. The plume persists until the complete disappearance of layer 1, which is slowly eroded through the entrained filaments (Fig. 2c), or until it reaches one of the vertical boundaries of the tank. The lifetime of such a plume ranged from 1 to 12 h, depending on the experimental conditions. This is observed on the whole range of Rayleigh numbers investigated (10^5–2.10^8) and regardless of whether layer 1 is more or less viscous than the convecting layer. The presence of layer 1 is therefore a very efficient way to anchor plumes for a long time.

In all the experiments, the final regime is a classical Rayleigh–Bénard convection in the whole tank (Fig. 3), with thermal plumes issuing from the top and bottom boundary layers.

2.3.2.2. Criteria for plume onset. Thermochemical plumes are generated through an instability of the stratified thermal boundary layer (Figs. 1b and 3). We therefore extend the phenomenological model of Howard [15] to a two-layer fluid. At the beginning of each experiment, the thermal boundary layer grows by conduction and its thickness δ increases with time (Figs. 4b and 5). We assume that convective instabilities emerge when a local Rayleigh number, based on the properties of the unstable part of the stratified boundary layer, exceeds a critical value Ra_c. Marginal stability analysis [26] has shown that: (1) for the buoyancy range of the experiments, we are always in the 'stratified' regime, and convection is going to develop first in the part of the thermal

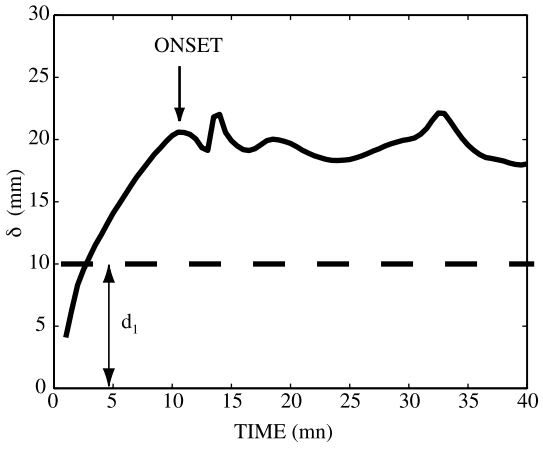

Fig. 5. Stratified thermal boundary layer thickness δ as a function of time. δ is defined as the height above the copper plate where the temperature decreases to 90% of the interior and surface temperatures [33]. It grows by heat diffusion until it becomes unstable. The dashed line shows the interface position at $t = 0$.

boundary layer which lies within layer 2, since layer 1 is too thin to convect on its own; (2) in the stratified regime, Ra_c does not depend on B but is a function of γ and d_1/δ. For each experiment, we therefore compute Ra_c [26] for the decreasing values of d_1/δ as time goes on (Table 1), and compare it to the local Rayleigh number in the unstable sublayer, based on its depth $\delta-d_1$ and the temperature drop across it: $\Delta T_B(1-d_1/\delta)$:

$$Ra_l = \frac{\alpha_{int} g \Delta T_B (\delta - d_1)^3}{\kappa \nu_2}\left(1-\frac{d_1}{\delta}\right). \quad (2)$$

Here, Ra_c ranges between the classical values for convection under a rigid slab (949) and an inviscid slab (530) of finite conductivity [26]. We can therefore predict a critical value of the boundary layer thickness at the onset of thermochemical plumes and compare it to the value measured in the experiment (Fig. 5). Table 1 summarizes our results. Calculated and measured boundary layer thicknesses agree quite well, especially for the high Rayleigh number cases.

In summary, for convection to develop, the thermal boundary layer has to grow thicker than if it was not stratified, since only the part above layer 1 becomes unstable (cf. [9,10,36,37]). This explains why the onset is delayed, compared to the purely thermal case.

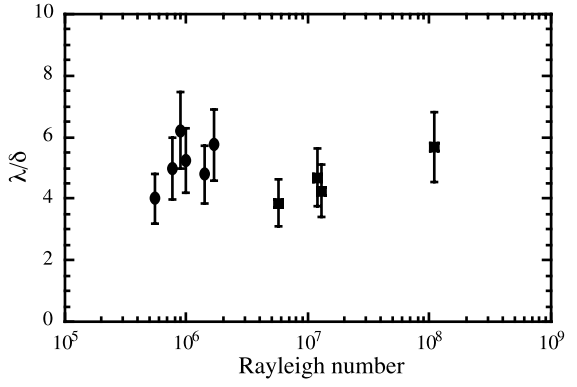

Fig. 6. Thermochemical plume averaged λ divided by the stratified boundary layer thickness δ, as a function of the Rayleigh number. The disks stand for the experiments with aspect ratio 5, while the squares stand for aspect ratio 2.

2.3.2.3. Wavelength and drift velocity. During an experiment, the number of thermochemical plumes did not change and was usually around 15, with distance between the plumes ranging from 6 to 12 cm (measured visually and on the horizontal probe). The resulting mean distance λ between the thermochemical plumes was difficult to evaluate because of the somewhat irregular polygonal geometry of the pattern and therefore the uncertainty is large (about 25%). λ was not observed to change significantly over the whole parameter range, and it did not depend on the aspect ratio of the tank. This might occur because the horizontal extent of the tank is too small to allow large variations of λ. However, since the thermochemical plumes form from boundary layer instabilities, we expect λ to be determined locally, and therefore to depend on δ. Now, δ varies only by 40% over the whole parameter range, which could explain why λ does not vary much either. For all our experiments, λ scales as (Fig. 6):

$$\lambda = (4.95 \pm 0.7) \times \delta \quad (3)$$

where δ is the thickness of the stratified thermal boundary layer averaged through time, once thermochemical plumes have started. It is interesting to note that λ is proportional to the whole stratified boundary layer thickness δ instead of being proportional only to the sublayer $\delta-d_1$. This is so because, as soon as convective instabilities start, layer 1 is deformed by them and the topography of the interface increases rapidly until it reaches a magnitude comparable to d_1: although the material from 1 is passively entrained by viscous coupling into 2, the whole thermal boundary layer participates to the dynamics. The topography of the interface induced by a thermochemical plume is also responsible for its strong anchorage: coupled with the strong plume thermal anomaly, it localizes the instability and forces the lateral flow in the thermal boundary layer along the cusp (Fig. 4d) [22,24,25].

The drift of the temperature anomalies associated with the plumes measured along the horizontal thermocouple probe ranged from 0.2 to 2 mm/min, with no systematics. As the probe was not

always parallel to the plume pattern drift, these values are indicative of the magnitude of the drift but are not the real values (our setup did not allow us to do better). Those values are one or two orders of magnitude smaller than the typical convective velocities in the tank (of typically a few cm/min). Non-dimensionalized by the convective velocity scale

$$\frac{\alpha g \Delta T d^2}{\nu_2} \tag{4}$$

they ranged from 6×10^{-6} to 1.4×10^{-4}. The motion between two plumes was even smaller, i.e. beyond the detection level.

2.3.2.4. Entrainment. Thermochemical plumes are local features. For instabilities to occur at the interface, temperature has to build up to overcome part of the stable chemical gradient. Let θ be the temperature anomaly associated with the thermochemical plume (Fig. 4c). Flow is generated by these lateral inhomogeneities of the interfacial temperature (Fig. 4d), with a characteristic thickness $\delta_p = \delta - d_1$ and a characteristic velocity W_p [8,25]. A filament of layer 1 is then entrained by viscous coupling with a thickness δ_e given by the balance between buoyancy forces and viscous forces [38]:

$$\alpha\theta g\delta_p - \frac{\Delta\rho}{\rho} g\delta_e \approx \nu \frac{W_p}{\delta_p} \tag{5}$$

This leads to the volumetric flux of entrained material across the interface [24,25]:

$$Q_m = C_1 \kappa\lambda B_l^{-2} Ra_P^{1/3} \frac{1}{1+\gamma/B_l} \tag{6}$$

where $B_l = \Delta\rho/(\rho\alpha\theta)$, $Ra_P = (\alpha g\theta\lambda^3/\kappa\nu_2)$, and C_1 is an experimental constant. The factor $1/(1+\gamma/B_l)$ in Eq. 6 reflects the fact that it is more difficult to entrain a viscous and/or strongly stratified fluid than an inviscid and/or weakly stratified one.

Experimentally, Q_m can be estimated by the time t_{end} necessary for one plume to completely erode the surrounding stratified boundary layer:

$$Q_m = \frac{d_1\lambda^2}{t_{end}} \tag{7}$$

Since the volume of layer 1 is small compared to the volume of layer 2, the variations with time of the physical properties of layer 2 (viscosity, thermal expansion, density) that enter Eq. 6 can be neglected throughout an experiment. We shall therefore take their values at $t=0$. The main uncertainty comes from the thermal expansion coefficient which strongly depends on temperature, and we shall take its value at the mean temperature through time of layer 2. In this case, Fig. 7 shows that Eq. 6 agrees well with the experimental results when $C_1 = (6.1\pm0.5)\times10^{-1}$ (this value is two orders of magnitude greater than the value given in [24] because there is a misprint in [24]). Moreover, the data shown contain two experiments where only Natrosol was used to change both density and viscosity along with data points obtained with salt–Natrosol–water solution. Although salt and Natrosol diffuse at very different rates, there is no discrepancy between the two sets of points; this proves that diffusion is not the

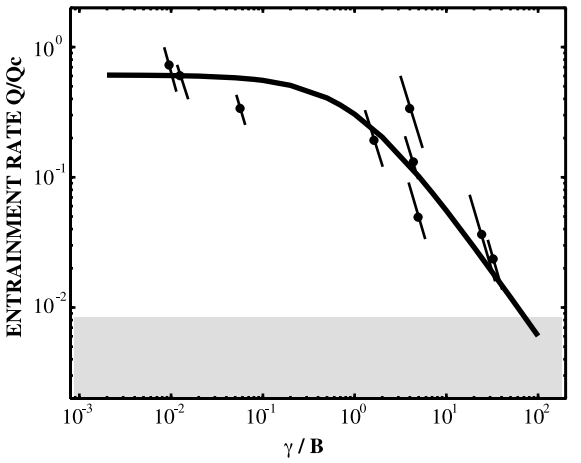

Fig. 7. Volumetric entrainment rate of a thermochemical plume divided by the convective scale as a function of γ/B. The circles represent the experimental measurements, while the solid line stands for Eq. 6. The shaded area shows the domain where salt diffusion becomes important.

mechanism of entrainment. A recent study by Gonnernam et al. [39], using different fluids (corn syrup and polybutene oils), also verifies the same law (Eq. 6).

We expect Eq. 6 to break down into four cases. (a) When the buoyancy ratio B_l tends towards 0, the convective regime changes from 'stratified' to 'whole layer' [24] and then the whole thin layer is flushed into the plumes. For $a > 5$, we observed this behaviour for $B < 0.3$ [26]. (b) When the buoyancy ratio tends towards infinity, i.e. when the density contrast is very high, or (c) when the entrained material is very viscous (γ tends toward infinity), the interface becomes increasingly difficult to deform and acts essentially the same as the flat boundaries at the top and bottom of the tank. In this case, the plumes should not be anchored anymore and should display the characteristics of a classical Rayleigh–Bénard convection (with a characteristic time scale given by Eq. 1) either on a rigid boundary (when $\gamma \gg 1$) or on a free boundary (when $\gamma \ll 1$). We were not able to observe these two limits b and c, because of salt diffusion [25], which becomes important when mechanical entrainment becomes too slow (shaded area in Fig. 7). (d) When the entrained fluid is much less viscous than the bulk fluid ($\gamma \ll 1$), it will resist entrainment by draining back into the cusp (Fig. 4d), and hence the thickness of entrained material should decrease for $\gamma/B \ll 1$. We were not able to observe this limit (Fig. 7).

The domain of validity of Eq. 6 is therefore at least $0.3 < B < 20$ for $10^{-2} < \gamma < 400$.

2.4. Results with $a < 5$

In this situation, both layers are convecting. Whenever $Ra > 10^5$ [26] and $B_l > B_c$, three-dimensional hot thermochemical plumes are observed in the less viscous layer (Fig. 1a,c). As for the case $a > 5$, they originate from thermal boundary layer instabilities developing on top of the bottom viscous cells, but get anchored by the coupling with the interface and the chemical heterogeneity. The interface can be either nearly flat (stratified regime of thermochemical convection, Fig. 1a) or highly distorted in a rising dome (oscillatory regime of thermochemical convection, Fig. 1c).

The entrainment rate through a plume was impossible to measure in the oscillatory regime because of the complexity of the convective pattern. However, measurements were made in the stratified regime [25]: since material was entrained both ways and more efficiently by two-dimensional structures in the more viscous layer than by three-dimensional plumes in the less viscous layer (as predicted analytically by Sleep [38]), the uncertainty on the mass flux entrained by the three-dimensional plumes was large and did not allow us to decipher any significant trend in cases where the viscosity ratio was increased. However, when these experiments are reanalysed using Eq. 6, they show a smaller standard deviation than previously determined ($\pm 10\%$ instead of $\pm 32\%$), and a behaviour consistent with data obtained for $a > 5$ (Fig. 7).

3. Anchored hotspots in a convecting mantle

3.1. Thermochemical plumes in a heterogeneous mantle

Thermochemical plumes appear in the stratified regime, i.e. whenever the buoyancy ratio is locally greater than a critical value B_c, weakly dependent on a and γ [26]. From the definition of the buoyancy ratio, thermochemical plumes therefore arise when the density contrast between the two layers is greater than:

$$\Delta\rho_c/\rho = \alpha_{int}\Delta T_B B_c \quad (8)$$

Fig. 8 shows $\Delta\rho_c/\rho$ as a function of ΔT_B for typical values of $B_c = 0.4$, and $\alpha_{int} = 3\times10^{-5}$ K^{-1} (typical for the transition zone), and 1×10^{-5} K^{-1} (deep mantle) [40]. Depending on where the thermochemical boundary layer is located, thermochemical plumes can be produced for the following density heterogeneities:

1. greater than 2% (e.g. point 'A' in Fig. 8) if the mantle is completely stratified with an interface in the mid-mantle (e.g. 670 km depth, Fig. 1a). According to seismic data, this situation seems precluded today.
2. greater than 0.2–0.3% (e.g. point 'B' in Fig. 8)

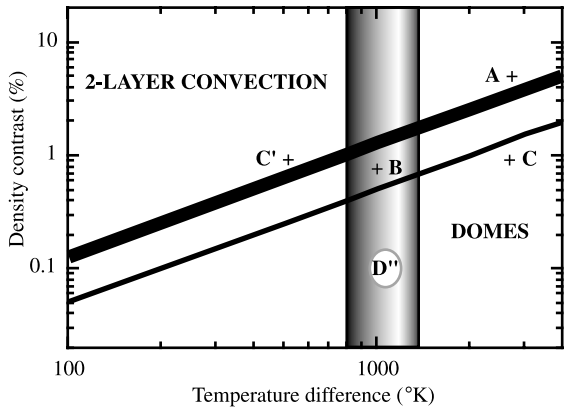

Fig. 8. Critical density contrast as a function of the temperature difference driving convection. The thin line dividing the two regimes is obtained for $\alpha = 10^{-5}$ K^{-1} and the thick line for $\alpha = 3\times10^{-5}$ K^{-1}. +A, whole mantle in the stratified regime; +B, locally stratified D″ layer; +C, whole mantle doming regime; +C′, locally stratified on top of a dome generated in +C.

if the interface lies in the D″ layer just above the core–mantle boundary (Fig. 1b, [36]).

3. around 0.1–1% (e.g. point 'C' in Fig. 8) if plumes form on top of a thermochemical 'dome' in the mid-mantle (Fig. 1c). This situation can occur either if the dome is rising, or if it is delayed (or even trapped) at the 670 phase transition on its way up to the surface (e.g. [41]). This latter case may apply to the Polynesian superswell [24].

In the mantle, density heterogeneities of such magnitude could be created by slab remnants (e.g. [42,43]), a relic of a 'primitive' mantle (e.g. [36,44,45]), a chemical reaction or infiltration from the core (e.g. [46], etc. So thermochemical plumes are expected to be common features in mantle convection (Fig. 9), and we suggest that they are responsible for long-lived hotspot volcanism.

3.2. Duration of a hotspot

In the experiments reported here, a thermochemical plume survives until its anchor, the thermochemical interface, disappears. This can happen in three different situations: (1) when the bottom layer has been completely drained throughout entrainment in the thermochemical plumes, (2) when the thermochemical dome from where the plumes were rising has reached the top boundary, or (3) if the rising thermochemical dome is stopped at the 670 km transition zone and, upon cooling, is collapsing back into the lower mantle.

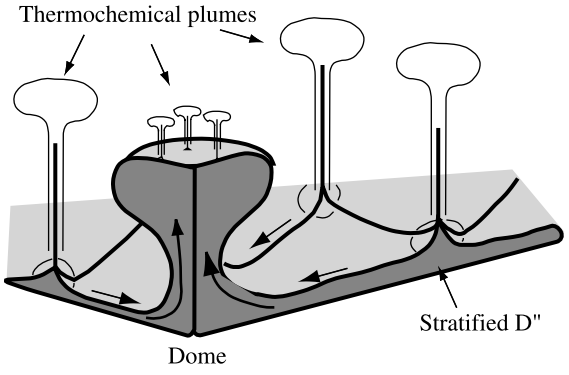

Fig. 9. Sketch of the thermochemical plume sources' motions induced by lateral motions in the stratified boundary layer. All plume sources are drifting towards the rising dome.

3.2.1. Thermochemical plumes out of a stratified D″: 'cold' hotspots

This would correspond to the first situation.

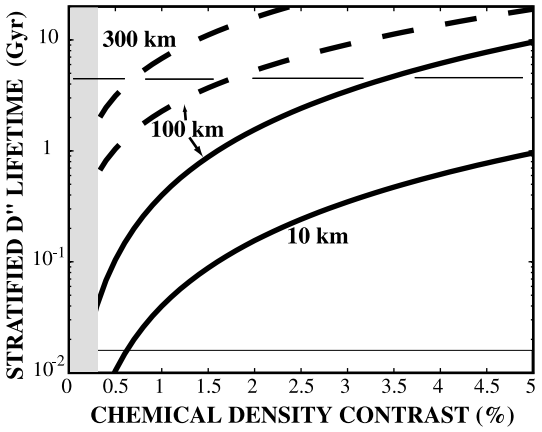

Fig. 10. Erosion time of a thin chemically different layer at the bottom of the mantle, as a function of the density heterogeneity for different layer thicknesses and different viscosity ratios (solid line, $\gamma = 1.0$; dashed line, $\gamma = 10$). The thin grey line represents the typical duration of a purely thermal plume calculated with Eq. 1 and Table 2. The shaded area shows the domain where the buoyancy ratio is below critical, i.e. where the system does not remain stratified.

Table 2
Parameters taken for the Earth's mantle

Depth of the mantle	d	2900 km
Density	ρ	4000 kg/m^3
Thermal expansion	α	10^{-5} K^{-1}
Thermal diffusivity	κ	10^{-6} m^2/s
Temperature heterogeneity	θ	500 K
Plume viscosity	η_2	10^{21} Pa·s

According to our experimental results (Section 2), the time needed to erode completely the denser part of D″ scales as:

$$t_{\mathrm{end}} = d_1 \frac{B^2}{C_1 \kappa}\left(1+\frac{\gamma}{B}\right)\left(\frac{\kappa \nu_2}{\alpha g \theta}\right)^{1/3} \quad (9)$$

Eq. 9 shows that the duration of a hotspot is independent of the wavelength λ and proportional to the heterogeneity thickness d_1. Fig. 10 shows the evolution of t_{end} as a function of the density heterogeneity for different viscosity ratios and thicknesses, using the mantle parameters given in Table 2. For these parameters, the typical duration of a purely thermal plume given by Howard's model (Eq. 1) would be around 16 Myr. This is smaller than the age of the Louisville or Hawaii hotspot tracks. Fig. 10 shows that the presence of density heterogeneities greatly increases the life of a plume, all the more if the heterogeneity is also more viscous than the bulk mantle. For a plume to live longer than 100 Myr, it would require to be anchored on a 100 km thick chemical heterogeneity of 0.5% or on a 10 km thick pile of 2% denser material (which could be former oceanic crust from a slab). Similarly, a 100 km thick heterogeneous layer inside D″ would survive over the age of the Earth for a density contrast greater than 2% if $\gamma = 10$, and greater than 3.5% if $\gamma = 1.0$. This latter value is comparable to the values obtained analytically by Sleep [38] and in numerical models by Tackley [36].

3.2.2. *'Weak' hotspots on an oscillating dome in the Pacific*

This would correspond to case '3'. In the Pacific, the Cretaceous Darwin Rise and the present-day 'superswell' beneath French Polynesia (see [47] for a review) are regions of anomalously shallow seafloor several thousands of kilometres in extent with an unusually dense concentration of hotspot tracks. Modelling based on correlation of seismic tomography, geoid and topography concludes that the Polynesian superswell is caused by dynamic upwelling of hot material in the mantle, and plate tectonics reconstructions show that, in the Cretaceous, the Darwin Rise was located where the Polynesian superswell is located today. These two features could therefore be created by a thermochemical dome with an oscillation period of about 80–100 Myr [24]. Since only volcanic tracks and small oceanic plateaus are seen on the superswells, it seems that, on its way to the surface, the dome has been trapped at the 670 km transition zone. In this case, the experiments predict generation of thermochemical plumes on top of the dome (Fig. 9). According to Eq. 3, their wavelength is proportional to the thickness of the thermal boundary layer at the top of the dome, which can be estimated to be 100–200 km. This would give a typical spacing between hotspots of 500–1000 km. Moreover, for an oscillation period of 80–100 Myr, the dome will remain at the transition zone for about 20% of that time before sinking back into the mantle [32], i.e. at most 20 Myr. This implies that the hotspot tracks generated on a thermochemical dome are short. On the Polynesian superswell, the volcanic chains are younger than 18 Myr and the inter-hotspot distance ranged from 800 to 1500 km [47]. Both the predicted spacing and the predicted short duration of the hotspots are coherent with these observations.

Both types of hotspots, 'cold' ones generated by thermochemical plumes out of a stratified D″ layer and 'weak' ones generated on top of a dome, can coexist on Earth (Fig. 9), depending on the magnitude of the density heterogeneities and of the depth dependence of thermal expansion.

3.3. *An Earth's mantle in two 'tanks'*

A strong signal of spherical harmonic degree two is always observed in worldwide geoid maps (e.g. [48]) and in the seismic tomography maps taken at different depths (e.g. [49]): the Earth's

mantle seems divided into two 'boxes' by the subducted plates, the Pacific box being isolated from the rest of the mantle by its subduction belt. It is therefore tempting to liken each of these mantle boxes to an experimental tank. In this light, our results may explain some features of the hotspots' distribution on Earth.

3.3.1. Hotspot motions within a tank

According to the experiments, the pattern of thermochemical plumes within each tank is expected to drift slowly to accommodate the vertical boundary conditions around each box. Eq. 4 and the typical values for Earth's parameters given in Table 2 give a drift velocity V between 10^{-2} and 1 mm/yr, and the inter-plume motions inside one box would be even less. The Indian and Atlantic hotspots have often been identified [2,3,50] as one group with inter-hotspot motion slower than the detection level (2–3 mm/yr). This inter-hotspot fixity in the Atlantic–Indian tank is expected from the experimental results.

3.3.2. Inter-tank motions

Since the geometries of the two mantle boxes are very different, there is no reason why the two hotspot groups should move coherently: we could observe a cumulate drift of up to $2\times V \leq 2$ mm/yr, i.e. at least an order of magnitude smaller than the observed 20 mm/yr. Now, the experimental results were obtained in the absence of plate tectonics and the 'mantle wind' which it creates. We are therefore looking at the motions of the sources of the hotspot plumes, which may be different from the motions of the hotspots on the surface. Indeed, Steinberger and O'Connell [20], assuming that the sources of the plumes were fixed, showed that the mantle wind caused all the Pacific hotspots to move more or less consistently towards the south–east, while hotspots in the Atlantic and Indian oceans are predicted to migrate independently from those in the Pacific, in agreement with the 20 mm/yr observed. Our experimental results explain why their hypothesis of plume source fixity was valid.

3.3.3. Inter-hotspot motions in the Pacific tank

A number of recent studies [51,52] have suggested that the Hawaiian hotspot migrated southwards from 68 to 43 Myr compared to the plate motion and had probably started doing so again 3–5 Myr ago. Now, we have shown that thermochemical plumes producing hotspots are anchored on a chemical layer deep in the mantle. If lateral motions are imposed to this layer by external causes such as impinging slabs [45] or a rising thermochemical dome [24], thermochemical plume anchor points are expected to move along. Thus current southward motion of Hawaii could be caused by the rise of the Pacific superswell (Fig. 9).

4. Conclusions

We have shown that the presence of a chemically stratified boundary layer generates long-lived thermochemical plumes. Although these plumes develop first from the interface as classical thermal boundary layer instabilities, they entrain by viscous coupling a thin film of the other layer and the interface deforms locally in cusps. The interfacial topography and the entrainment act to further anchor the plumes, which persists until the chemical stratification disappears through entrainment, even for Rayleigh numbers around 10^8. The pattern of thermochemical plumes remains the same during an experiment. Scaled to an Earth's mantle without plate tectonics, our results show that: (1) thermochemical plumes are expected to exist in the mantle; (2) they could easily survive hundreds of millions of years, depending on the size and the magnitude of the chemical heterogeneity on which they are anchored; (3) their drift velocity would be at most 1–2 mm/yr. They would therefore produce long-lived hotspots on the lithosphere, and these hotspots could remain relatively fixed. However, it is worth noting that the chemical heterogeneity acts more as a 'floating anchor' than as an absolute one, since the thermochemical plumes would follow any large scale motion imposed on the chemical layer. Therefore, the fact that Earth's hotspots are relatively fixed compared to tectonic plates gives us an important constraint on the physics of plate tectonics: there must be a physical phenomenon at play in the mantle which decouples plate motions from

the thermochemical layer on which the hotspot plumes are anchored.

Acknowledgements

We benefitted from discussions with Alain Bonneville, Cinzia Farnetani, Claude Jaupart, Henri-Claude Nataf and Neil Ribe. The manuscript was improved thanks to the constructive reviews of Peter Olson and Paul Tackley and the comments of Michael Manga and Vincent Courtillot. The help in the laboratory of G. Bienfait, C. Carbonne, A. Lee and W. Phelps is gratefully acknowledged. Part of this work was done at the Department of Geology at Yale University, New Haven, CT, USA.*[AC]*

References

[1] J.T. Wilson, Evidence from islands on the spreading of the ocean floor, Can. J. Phys. 41 (1963) 863–868.
[2] P. Molnar, J. Stock, Relative motions of hotspots in the Pacific, Atlantic and Indian Oceans since late Cretaceous time, Nature 327 (1987) 587–591.
[3] R.A. Duncan, M.A. Richards, Hot spots, mantle plumes, flood basalts, and true polar wander, Rev. Geophys. 29 (1991) 31–50.
[4] W.J. Morgan, Plate motions and deep mantle convection, Nature 230 (1971) 42–43.
[5] J.A. Whitehead, D.S. Luther, Dynamics of laboratory diapir and plume models, J. Geophys. Res. 80 (1975) 705–717.
[6] P. Olson, H. Singer, Creeping plumes, J. Fluid Mech. 158 (1985) 511–531.
[7] R.E. Griffiths, I.H. Campbell, Stirring and structures in mantle starting plumes, Earth Planet. Sci. Lett. 99 (1990) 66–78.
[8] P. Olson, G. Schubert, C. Anderson, Structure of axisymmetric mantles plumes, J. Geophys. Res. 98 (1993) 6829–6844.
[9] M. Albers, U.R. Christensen, The excess temperature of plumes rising from the core-mantle boundary, Geophys. Res. Lett. 23 (1996) 3567–3570.
[10] C.G. Farnetani, Excess temperature of mantle plumes: the role of chemical stratification across D″, Geophys. Res. Lett. 24 (1997) 1583–1586.
[11] N.H. Sleep, Hotspots and mantle plumes: some phenomenology, J. Geophys. Res. 95 (1990) 6715–6736.
[12] P. Olson, Hot spots, swells and mantle plumes, in: M.P. Ryan (Ed.), Magma Transport and Storage, Wiley, New York, 1990, pp. 33–51.
[13] M.A. Richards, R.A. Duncan, V.E. Courtillot, Flood basalts and hot-spot tracks: plume heads and tails, Science 246 (1989) 103–107.
[14] N.H. Sleep, M.A. Richards, B.H. Hager, Onset of plumes in the presence of preexisting convection, J. Geophys. Res. 93 (1988) 7672–7689.
[15] L.N. Howard, Convection at high Rayleigh number, in: H. Görtler (Ed.), Proc. 11th Int. Congr. Applied Mechanics, Springer, Berlin, 1964, pp. 1109–1115.
[16] N. Schaeffer, M. Manga, Interaction of rising and sinking mantle plumes, Geophys. Res. Lett. 21 (2001) 765–768.
[17] S. Labrosse, Hotspots, mantle plumes and core heat loss, Earth Planet. Sci. Lett. 199 (2001) 147–156.
[18] J.A. Whitehead, Instabilities of fluid conduits in a flowing Earth – are plates lubricated by the asthenosphere?, Geophys. J. R. Astron. Soc. 70 (1982) 415–433.
[19] M.A. Richards, R.W. Griffiths, Deflection of plumes by mantle shear flow: experimental results and a simple theory, Geophys. J. 94 (1988) 367–376.
[20] B. Steinberger, R.J. O'Connell, Advection of plumes in mantle flow: implications for hotspots motion, mantle viscosity and plume distribution, Geophys. J. Int. 132 (1998) 412–434.
[21] U. Hansen, D.A. Yuen, S.E. Kroening, T.B. Larsen, Dynamical consequences of depth-dependent thermal expansivity and viscosity on mantle circulations and thermal structure, Phys. Earth Planet. Int. 77 (1993) 205–223.
[22] A. Namiki, K. Kurita, The influence of boundary heterogeneity in experimental models of mantle convection, Geophys. Res. Lett. 26 (1999) 1929–1932.
[23] A.W. Hofmann, Mantle geochemistry: the message from oceanic volcanism, Nature 385 (1997) 219–229.
[24] A. Davaille, Simultaneous generation of hotspots and superswells by convection in a heterogeneous planetary mantle, Nature 402 (1999) 756–760.
[25] A. Davaille, Two-layer thermal convection in miscible viscous fluids, J. Fluid Mech. 379 (1999) 223–253.
[26] M. LeBars, A. Davaille, Stability of two layer convection in viscous fluids, J. Fluid Mech. (2002) in press.
[27] U. Christensen, Instability in a hot boundary layer and initiation of thermo-chemical plumes, Ann. Geophys. 2 (1984) 311–320.
[28] F. Girard, A. Davaille, Dynamics of an heterogeneous layer at the base of the mantle: an experimental approach, EOS 79 (1998) 617.
[29] R. Krishnamurti, On the transition to turbulent convection, J. Fluid Mech. 42 (1970) 295–320.
[30] F.M. Richter, D.P. McKenzie, On some consequences and possible causes of layered convection, J. Geophys. Res. 86 (1981) 6133–6134.
[31] P. Olson, An experimental approach to thermal convection in a two-layered mantle, J. Geophys. Res. 89 (1984) 11293–11301.
[32] M. LeBars, A. Davaille, Large deformations of the interface in two-layer thermal convection of miscible viscous fluids at high Rayleigh number, J. Fluid Mech. (2002) submitted.

[33] N. Tamai, T. Asaeda, Sheetlike plumes near a heated bottom plate at large Rayleigh number, J. Geophys. Res. 89 (1984) 727–734.
[34] T. Asaeda, K. Wanatabe, The mechanism of heat transport in thermal convection at high Rayleigh numbers, Phys. Fluids A1 5 (1989) 861–867.
[35] G.A. Houseman, The thermal structure of mantle plumes: axisymmetric or triple-junction?, Geophys. J. Int. 102 (1990) 25–43.
[36] P.J. Tackley, Three-dimensional simulations of mantle convection with a thermo-chemical basal boundary layer: D″? in: The Core-Mantle Boundary Region, AGU Monogr., Am. Geophys. Union, Washington, DC, 1998, pp. 231–255.
[37] N.L. Montague, L.H. Kellogg, M. Manga, High Rayleigh number thermo-chemical models of a dense boundary layer in D″, Geophys. Res. Lett. 25 (1998) 2345–2348.
[38] N.H. Sleep, Gradual entrainment of a chemical layer at the base of the mantle by overlying convection, Geophys. J. 95 (1988) 437–447.
[39] H.M. Gonnermann, M. Manga, A.M. Jellinek, Dynamics and longevity of an initially stratified mantle, Geophys. Res. Lett. 29 (2002) paper 10.1029/2002GL01485.
[40] A. Chopelas, R. Boehler, Thermal expansivity in the lower mantle, Geophys. Res. Lett. 19 (1992) 1983–1986.
[41] P.J. Tackley, On the penetration of an endothermic phase transition by upwellings and downwellings, J. Geophys. Res. 100 (1996) 15477–15488.
[42] P. Olson, C. Kincaid, Experiments on the interaction of thermal convection and compositional layering at the base of the mantle, J. Geophys. Res. 96 (1991) 4347–4354.
[43] U.R. Christensen, A.W. Hofmann, Segregation of subducted oceanic crust in the convecting mantle, J. Geophys. Res. 99 (1994) 19867–19884.
[44] M. Gurnis, G.F. Davies, The effect of depth-dependent viscosity on convective mixing in the mantle and the possible survival of primitive mantle, Geophys. Res. Lett. 13 (1986) 541–544.
[45] L.H. Kellogg, B.H. Hager, R.D. van der Hilst, Compositional stratification in the deep mantle, Science 283 (1999) 1881–1884.
[46] U. Hansen, D.A. Yuen, Numerical simulations of thermo-chemical instabilities at the core-mantle boundary, Nature 334 (1988) 237–240.
[47] M.K. McNutt, Superswells, Rev. Geophys. 36 (1998) 211–244.
[48] A. Cazenave, A. Souriau, K. Dominh, Global coupling of Earth surface topography with hotspots, geoid and mantle heterogeneities, Nature 340 (1989) 54–57.
[49] R.D. van der Hilst, S. Widiyantoro, E.R. Engdahl, Evidence for deep mantle circulation from global tomography, Nature 386 (1997) 578–584.
[50] D.M. Müller, J.Y. Royer, L.A. Lawyer, Revised plate motions relative to the hotspots from combined Atlantic and Indian Ocean hotspot tracks, Geology 21 (1993) 275–278.
[51] I.O. Norton, Plate motion in the North Pacific the 43 ma non-event, Tectonics 14 (1995) 1080–1094.
[52] J.A. Tarduno, R.D. Cotrell, Paleomagnetic evidence for motion of the Hawaiian hotspot during formation of the Emperor Seamounts, Earth Planet. Sci. Lett. 153 (1997) 171–180.